



## Random Macropore Formation in p-Type Silicon in HF-Containing Organic Solutions

### Host Matrix for Metal Deposition

Farid A. Harraz,<sup>a,b</sup> Kentaro Kamada,<sup>a</sup> Katsutoshi Kobayashi,<sup>a</sup> Tetsuo Sakka,<sup>a,\*</sup> and Yukio H. Ogata<sup>a,\*z</sup>

<sup>a</sup>Institute of Advanced Energy, Kyoto University, Uji, Kyoto 611-0011, Japan

<sup>b</sup>Advanced Materials Technology Department, Central Metallurgical Research and Development Institute, Helwan, Cairo 11421, Egypt

Random macropore formation in variously doped p-type silicon substrates (0.01–20  $\Omega$  cm) by electrochemical anodization in aqueous HF-containing dimethylsulfoxide, dimethylformamide, or acetonitrile was investigated under different operating conditions. A systematic study of the effect of the main parameters controlling the macropore formation is reported. The results revealed that the nature of organic solvent, the concentration of HF, and the substrate doping level play major roles in determining pore formation and morphology. Also, the behavior of these macropores in contact with an aqueous solution of  $\text{Ag}_2\text{SO}_4$  in the dark and at room temperature is investigated and a possible reaction mechanism for the deposition process is proposed.  
© 2005 The Electrochemical Society. [DOI: 10.1149/1.1864292] All rights reserved.

Manuscript submitted August 5, 2004; revised manuscript received September 6, 2004. Available electronically March 9, 2005.

The electrochemical etching of silicon in HF-based solutions is known to form a porous layer on the surface.<sup>1,2</sup> The dimensions of these pores are tiny and mostly located in the nanometer-scale range.<sup>3,4</sup> Recently, the formation of macropores (pores in the micrometer-size diameter range) has attracted increasing interest because of their promising features for a wide scope of applications such as microelectromechanical systems (MEMS),<sup>5–7</sup> sensors,<sup>8,9</sup> and biotechnology.<sup>10</sup> Furthermore, Lehmann and Rönnebeck reported in a recent work<sup>11</sup> that macropores filled with lead can produce X-ray filters. Lévy-Clément and co-workers<sup>12,13</sup> extensively studied the use of macropores prepared on p-type Si in organic solutions as antireflection layers on polycrystalline solar cells. One of the prominent applications of macropores is in the field of photonic bandgap materials, so-called photonic crystals<sup>14,15</sup> in which a periodic variation of the refractive index in the submicrometer range (a scale matched to the wavelength of light) is fabricated. In the current study, we show that p-type macropores can be also used as templates for introduction of noble metal deep into the pores. This process can produce novel composite structures from macroporous silicon.

The first macroporous structure prepared on n-type Si substrates was observed by Theunissen in 1972<sup>16</sup> in aqueous HF solution and was investigated in detail in the 1990s.<sup>17,18</sup> However, Propst and Kohl reported the first experiments of macropore formation on p-type Si only in 1994.<sup>19</sup> They used anhydrous HF in acetonitrile and moderately doped p-type substrates. Later on, further studies showed the possibility to obtain macropores on p-type Si either in aqueous HF<sup>20</sup> or aqueous HF-containing organic solutions.<sup>21</sup>

While macropore formation in n-type Si is well explained in terms of the space charge region (SCR), which leads to a collection of the photogenerated carriers at the pore tips,<sup>22</sup> pore formation in p-type electrodes is controversial. In contrast to n-type Si, p-type substrate (in the anodic regime) is now under the forward bias condition. Propst and Kohl,<sup>19</sup> who first observed the macropores on p-type Si, attributed their results to specific chemical processes. Later, several mechanisms have been invoked to explain the macropore formation in p-type Si. Of particular importance are the depletion and field effects model,<sup>23</sup> the chemical passivation model,<sup>21</sup> the linear stability model,<sup>24</sup> the current burst model,<sup>25</sup> and the pure chemical model.<sup>26</sup> In the depletion and field effects model, charge-transfer mechanisms across the Schottky barrier are proposed. The chemical passivation model explains macropore formation as a result of adsorption of organic molecules on the silicon

electrodes, which in turn changes the way of silicon dissolution. The main idea of the linear stability model is that the formation of macropores occurs only if a certain ratio of electrolyte and substrate resistivities is achieved; however, the model is further modified with new assumptions.<sup>27</sup> The current burst model postulates that the charge transfer at the Si/electrolyte interface is spatially and temporally inhomogeneous. Finally, the pure chemical model gives an explanation based on chemical kinetics for pore initiation during the anodic dissolution of n-type Si in HF solution, which can be applied to p-type Si as well. According to this model, the silicon surface is dissolved anodically to the Si(I) intermediate which is very mobile and acts as a catalyst for the dissolution reaction. However, none of the above-mentioned models can explain all the experimental data available in the literatures. Furthermore, a definite understanding of the limits of pore formation and morphologies are not available for p-type substrates.

Ordered pore arrays on Si are usually fabricated by applying a multistage process including the photolithographic patterning and subsequent alkaline etching.<sup>18,28</sup> If the preparation of such well-ordered pore alignments without pre-etching could be achieved, it would be fascinating. Hence, basic understanding of random pore formation is important.

Many organic solvents have been usually mixed with HF during the macropore formation in p-type silicon. Of these, dimethylsulfoxide (DMSO), dimethylformamide (DMF), and acetonitrile (MeCN) are the most frequently investigated and are used in this study. Further, this series of solvents in addition to the EtOH have different physicochemical properties and hence, different effects during pore formation are expected.

In this paper, a systematic study of the effect of the main parameters controlling the macropore formation, such as substrate doping level, HF concentration, type of organic solvent, applied current density, and anodization time, is reported. Then, the use of such macropores as a “host matrix” for the impregnation of Ag metal by a simple immersion plating technique in the dark and at room temperature is presented.

### Experimental

The Si(100) single crystals used in this study were p-type boron-doped with different resistivities: 0.01–0.02, 0.1–0.2, 3.2–4.8, and 10–20  $\Omega$  cm, corresponding to doping densities of  $7 \times 10^{18}$ ,  $1 \times 10^{17}$ ,  $8 \times 10^{15}$ , and  $1 \times 10^{15}$   $\text{cm}^{-3}$ , respectively. All wafers were mirror-polished (without etch pits) with 0.6 mm thickness, pre-treated in acetone, and afterward dipped in 5 wt% HF to remove the native oxide layer.

The electrochemical anodization was performed galvanostati-

\* Electrochemical Society Active Member.

<sup>z</sup> E-mail: y-ogata@iae.kyoto-u.ac.jp

cally in a cell made of trifluoroethylene resin using a two-electrode setup with a Pt rod serving as a counter electrode. The exposed surface area of the Si electrode was  $0.785 \text{ cm}^2$ , adjusted by using an O-ring at the bottom of the cell. The electrolyte was a mixture of aqueous HF (47 wt%) and the following organic solvents: DMSO, DMF, or MeCN. Different concentrations of HF were used from 2 to 10 M (3-17 wt%). Tetra-*n*-butylammonium perchlorate (TBAP) as a supporting electrolyte was added in appropriate concentrations. The current density was varied from 2 to  $50 \text{ mA/cm}^2$  for anodization time from 4 min to 3 h.

Current-potential curves were measured using an automatic polarization system HZ-3000, Hokuto Denko. A three-electrode cell was used with an Ag/AgCl electrode as a reference and a Pt wire as a counter electrode. The ohmic contact on the rear side between Si electrode and a Cu current collector was achieved by rubbing Ga-In eutectic alloy.

Surface topography using a pin-type Tencor P-10 profilometer was performed for some macroporous samples. Scan speed of  $0.4 \text{ mm/s}$ , horizontal resolution of  $8 \mu\text{m}$ , vertical resolution of  $0.2 \text{ nm}$ , maximum vertical full scale of  $150 \mu\text{m}$ , and stylus force of  $5 \text{ mg}$  were the main line scan parameters.

The macroporous layer formed in aqueous HF/DMSO solution was immersed for 60 min in an aqueous solution of  $5 \times 10^{-3} \text{ M}$   $\text{Ag}_2\text{SO}_4$  in the dark at room temperature. After the immersion, the samples were rinsed in pure water and dried by blowing Ar gas. An Elionix model ERA-800 field emission-type scanning electron microscope (FE-SEM) was used for structure evaluation. X-ray diffraction patterns (XRD) were measured on a Rigaku RAD 2C system with an attachment for thin-film measurement. The radiation source was Cu  $\text{K}\alpha$  ( $1.54 \text{ \AA}$ ) with a data acquisition rate of  $1 \text{ deg/min}$ .

### Results and Discussion

**Current-potential behavior.**—Figure 1A shows the current-potential behavior of a  $10\text{-}20 \Omega \text{ cm}$  p-type Si at scan rate of  $10 \text{ mV/s}$  in solutions containing  $4 \text{ M}$  HF +  $0.1 \text{ M}$  TBAP in MeCN, water, DMF, and DMSO. A typical current density-potential (*i*-*E*) response with a current peak is obtained in aqueous HF solution (curve b). The region at the initial rising part is related to porous silicon layer formation, followed by a passivating region due to the anodic oxidation of the substrate. At a potential higher than  $6 \text{ V}$  (vs. Ag/AgCl), current oscillation is observed which is attributed to the breakage and repair of the oxide layer in the presence of HF solution.<sup>29</sup> In the solution containing DMSO (curve d), the current peak and oscillation are also observed but less pronounced and occur at a lower current value compared to the pure aqueous HF solution. In HF/DMF solution (curve c) the current peak is shifted to a higher potential and is reduced to a broad shoulder, which has a higher current than the case of DMSO solution. We think that the current peak is there but may be hidden due to either the high scan rate or the high electrolyte resistivity. This is further clarified by performing the same experiments at a lower scan rate of  $1 \text{ mV/s}$ , and the results are depicted in Fig. 1B. The current peak in DMF solution (curve c) is now obvious and the oscillation is also detected.

On the contrary, the *i*-*E* behavior in the MeCN-containing solution (Fig. 1A, curve a) is quite different. The current rises almost linearly with the applied potential, exhibits a small hump at around  $2 \text{ V}$  (vs. Ag/AgCl), and then increases again up to  $200 \text{ mA/cm}^2$  (the maximum current scale is not shown). The appearance of such a hump is clear in curve a of Fig. 1B. At the beginning of the initial part before the hump, a porous layer is formed. After the hump, electropolishing of Si occurs. The hump position, current density and potential, is determined by the kinetics at the interface. Diffusion of reactants affects the current density at high potential but within the porous formation region, and therefore a fast scan makes the rate higher. Furthermore, the morphology may affect the transport phenomena. Hydroxide and/or oxide formation is considered to take part in the electropolishing process, although the formation appears as an intermediate state. The balance of these above pro-

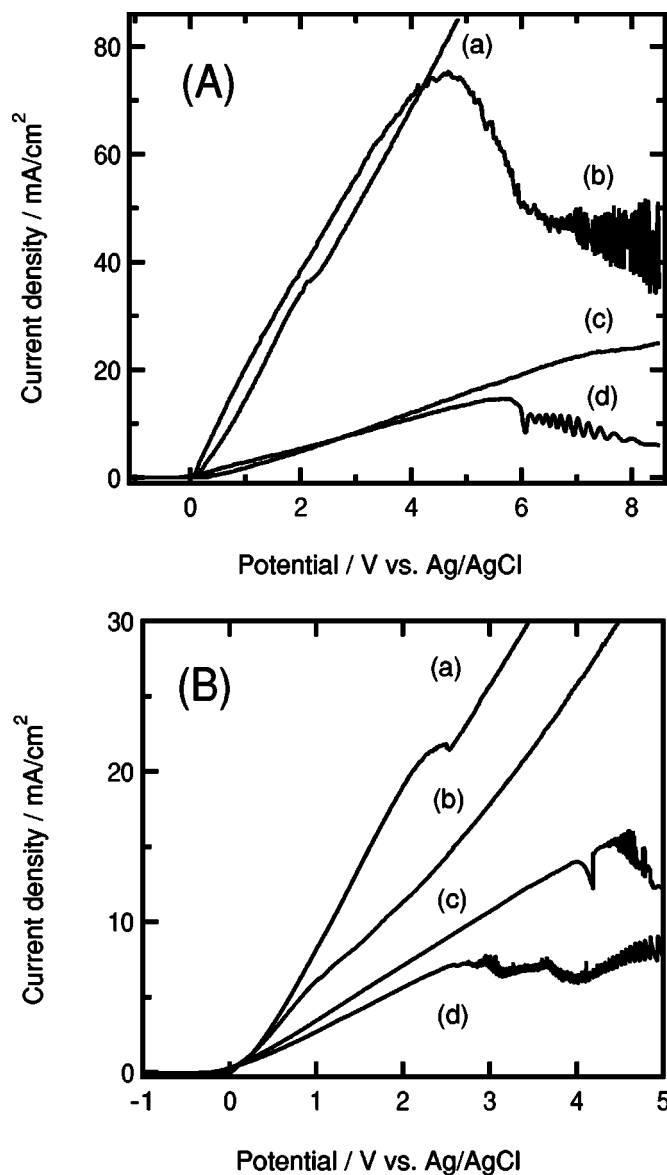


**Figure 1.** Current density-potential curves: (A) for a  $10\text{-}20 \Omega \text{ cm}$  p-type Si at scan rate of  $10 \text{ mV/s}$  in solutions containing  $4 \text{ M}$  HF +  $0.1 \text{ M}$  TBAP mixed with (a) MeCN, (b)  $\text{H}_2\text{O}$ , (c) DMF, and (d) DMSO. (B) is the same as (A), except that the scan rate was  $1 \text{ mV/s}$  and (curve b) is for EtOH solution.

cesses determines the hump position. Here a fast scan favors the increase of the critical current density, as can be seen in curve a of Fig. 1A compared to curve a of Fig. 1B.

In using HF in EtOH instead of water (curve b in Fig. 1B), the current rises with the electrode potential up to  $33 \text{ mA/cm}^2$  and a current peak typical for aqueous solution is not observed within this potential range. This means that the porous silicon is still formed and no passivation is detected under this condition in this ethanol-based solution.

**Macropore formation in different types of organic solvents.**—Macroporous structures in all samples under various conditions ( $2\text{-}50 \text{ mA/cm}^2$  and  $2\text{-}10 \text{ M}$  HF) were not observed either in pure aqueous or ethanolic solutions containing HF, however, nanoporous layers were formed instead. The presence of an organic solvent in the electrolyte during the macropore formation in p-type Si is essential in this work. In all electrolytes we observed the evolution of hydrogen gas during the anodization process. Top and cross-sectional views of FE-SEM images after the galvanostatic treatment

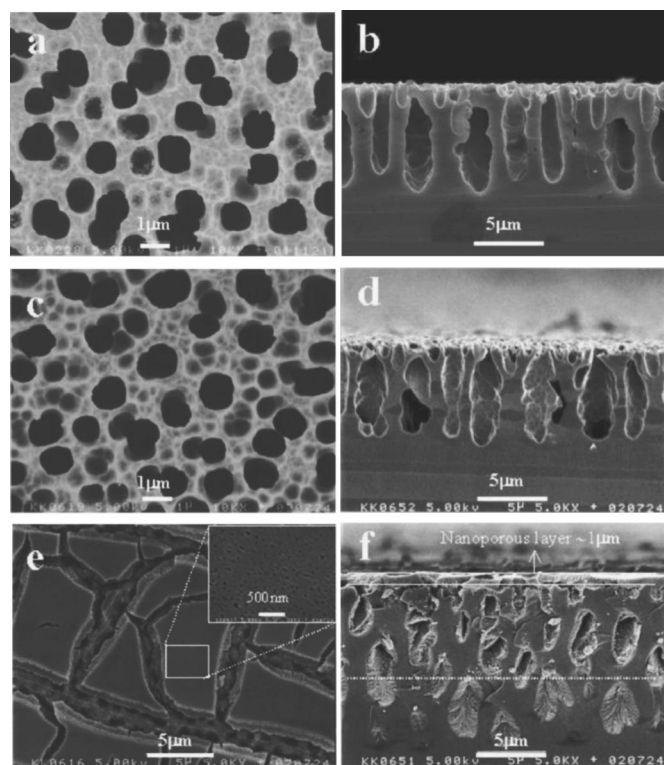


**Figure 2.** Top (left) and cross-sectional view (right) FE-SEM micrographs of macropores formed by an electrochemical etching in a 10–20  $\Omega$  cm p-type Si at 2 mA/cm<sup>2</sup> for 60 min in 4 M HF containing different organic solvents: (a, b) DMSO, (c, d) DMF, and (e, f) MeCN.

of the 10–20  $\Omega$  cm samples in a 4 M HF with DMSO, DMF, and MeCN are shown in Fig. 2. The applied current density and the anodization time were 2 mA/cm<sup>2</sup> and 60 min, respectively. In the HF/DMSO and HF/DMF solutions, round macropores approximately 1  $\mu$ m in diameter and 7  $\mu$ m in depth are formed (Fig. 2a–d). The pores show almost the same depth and grow parallel to each other. The parallel growth of pores is related to the passivating behavior of the pore walls.<sup>27</sup> The images shown in Fig. 2a–d reveal also that most of the pore volume obtained in both electrolytes is empty. However, we show that a thin nanoporous layer is also there.

In contrast, a bilayer structure is formed in the HF/MeCN solution, which is considerably different from that obtained in HF/DMSO or HF/DMF solutions. A thin nanoporous layer, about 1  $\mu$ m thick, is formed at the top of the surface with a macroporous layer beneath it (see Fig. 2e and f). This nanoporous layer cracks upon drying, revealing macropores below it, as can be seen in the top view image. A similar kind of nanoporous layer formation during the macropore formation on a moderately doped p-type substrate using HF/MeCN<sup>21</sup> or HF/MeCN containing diethyleneglycol solutions<sup>30</sup> has been reported.

In the cross-sectional view of Fig. 2f, the macroporous layer depth obtained in MeCN solution is approximately 11  $\mu$ m and is mainly filled with nanopores. Above the dotted line in the image, empty macropores are observed, whereas filled macropores are still there under the line. In addition, the pores are intermittent, probably because the pore growth direction is not perfectly perpendicular to the surface. This tortuous way of growth might enhance the tendency to branching in this solution.

The topographic profiles of the macropores formed in these organic solvents are shown in Fig. 3. The surface profiles were found to depend on the solvent used. In the MeCN solution, the surface of the macroporous layer has almost the same level as that of the untreated wafer. This is in consistent with the smooth surface appear-

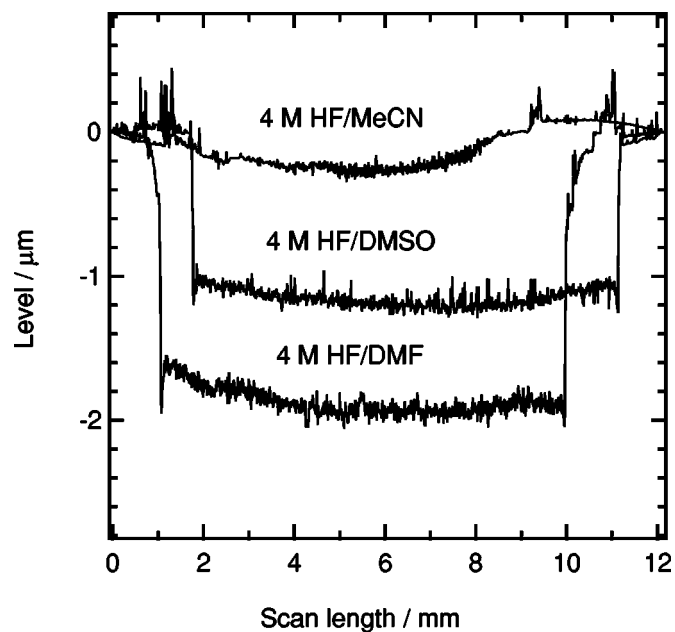


**Figure 3.** Topographic profiles of the macroporous silicon prepared in a 4 M HF solution with different organic solvents. The current density and the anodization time were 2 mA/cm<sup>2</sup> and 60 min, respectively.

ing in the FE-SEM image of Fig. 2f. However in DMSO or DMF solutions, an around 1 or 2  $\mu$ m deep profile is observed, respectively. This result implies that a nanoporous layer might also be formed in DMSO or DMF, then chemically attacked and subsequently dissolved in both solutions; rough surfaces are observed in FE-SEM images of Fig. 2b and d. It has also been demonstrated experimentally that pure DMSO<sup>31</sup> and both DMSO and DMF<sup>32</sup> could react chemically with the nanoporous silicon. This assumption is supported by the observation of progressive transition from a homogeneous nanoporous layer to macropores during pore formation in organic solutions.<sup>24,27</sup>

Based on this observation, the solvent type and effect can be classified into three categories: (i) DMSO and DMF favor macropore formation, (ii) MeCN gives a bilayer of nano/macropores, and (iii) aqueous and ethanolic solutions lead to the formation of nanopores. Now a question arises to understand the different behavior of these solvents during the pore formation. According to Lust and Levy-Clement,<sup>33,34</sup> the different effects are attributed to the different solution chemistry, which in turn affects and controls the rate of chemical and electrochemical reactions taking place during the anodic dissolution of silicon in HF solution. They considered the different protic character (acid-base properties) of the solvents to account for the different behavior of water and ethanol on one side and DMSO, DMF, and MeCN on the other side. Water and ethanol are protic, *i.e.*, strong hydrogen-bond donors, and hence, anions are much more stable there. DMSO, DMF, and MeCN are aprotic solvents as they exchange protons very slowly. This means that the anions, *e.g.*, F<sup>-</sup> and HF<sub>2</sub><sup>-</sup>, are very mobile in these solvents and consequently enhance the silicon dissolution rate. The different effects between DMSO and DMF as one group and MeCN as another group are related to their different donor or solvating properties. As it has been also proposed in Ref. 33 and 34, the oxidizing properties, the redox potential, the build-in potential, and the solubility of the reaction products may have effects on the different behaviors of the solvents.

As mentioned previously, we could not obtain macropores in HF solutions with either water or ethanol. However, Lehmann and Rönnebeck<sup>23</sup> reported that the presence of an organic solvent in the electrolyte is not essential for macropore formation on p-type Si. They observed macropores in aqueous HF solution for substrate

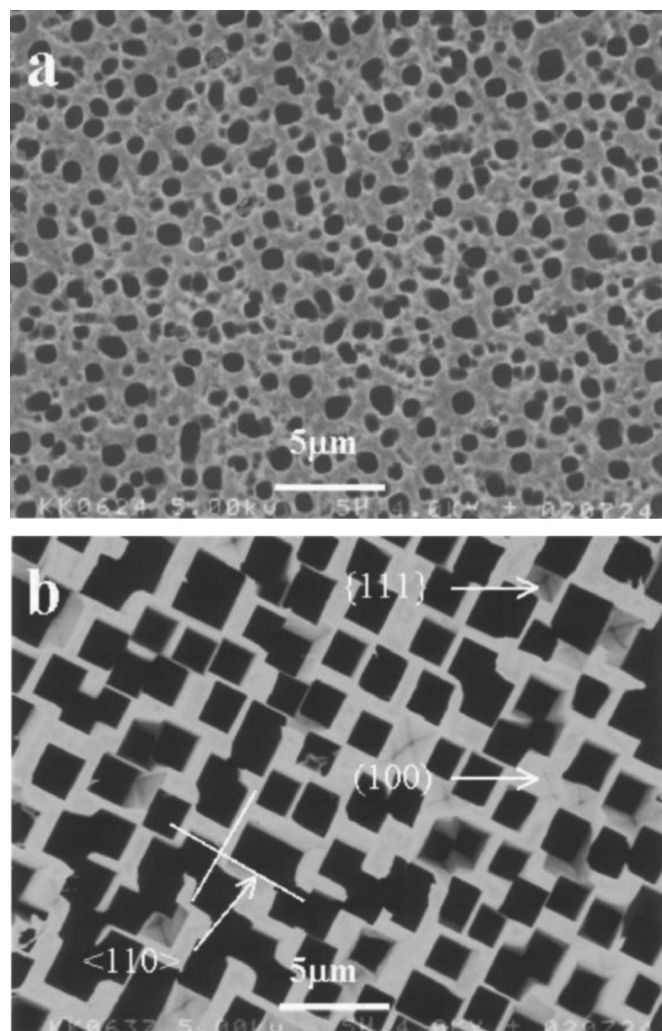


**Figure 4.** Top-view FE-SEM images of macropores formed in 10-20  $\Omega$  cm p-type Si at 10 mA/cm<sup>2</sup> for 20 min in a 4 M HF/DMSO solution: (a) as-anodized sample and (b) after immersion in 0.1 M KOH for 30 min.

resistivity above 5  $\Omega$  cm. They used prepatterned substrates with etch pits; however, our samples are mirror-polished without etch pits. The presence of such etch pits certainly favors Si dissolution and pore formation.

If the macropores are immersed in an alkaline solution of KOH, the nanoporous body is dissolved with the evolution of hydrogen gas. Figure 4a and b, for example, shows top-view FE-SEM micrographs of macropores prepared in HF/DMSO solution before and after immersion in 0.1 M KOH for 30 min, respectively. After the immersion, the round macropores are found to convert to square shape and the average pore sizes widened nearly twice. In this solution, chemical etching occurs, which is an orientation-dependent process.<sup>35</sup> The overall etch rate of the sample under this condition is 0.077  $\mu$ m/min. The (111) plane is the most resistant to etching compared to the other crystal orientations.<sup>35</sup> It seems that during the etching the (100) plane starts to disappear gradually, leaving the (111) crystal faces behind, and this is the reason for the morphology changes.

Based on this investigation, we conclude that the pore morphology and orientation are strongly dependent on the type of organic solvent added to the electrolyte. The presence of the nanoporous body with the macroporous structure in the MeCN solution indicates that the current density at the macropore tip is below the critical

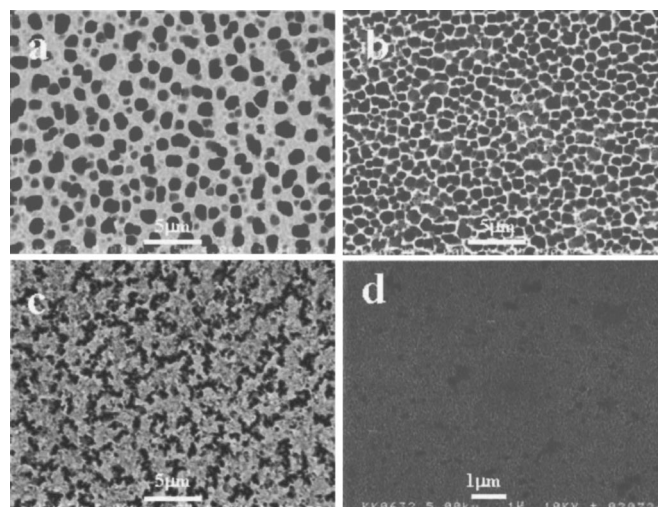


**Figure 5.** Top-view FE-SEM micrographs of macropores obtained in 4 M HF/DMSO at 2 mA/cm<sup>2</sup> for 60 min using p-type Si of different resistivities: (a) 10-20, (b) 3.2-4.8, (c) 0.1-0.2, and (d) 0.01-0.02  $\Omega$  cm.

current density and hence the electropolishing regime is never reached. Under identical conditions, better pore formation and morphology are observed in DMSO- and DMF-based solutions in comparison to the MeCN-containing HF.

**Substrate doping density.**—The influence of the doping level (0.01-20  $\Omega$  cm,  $7 \times 10^{18}$  to  $10^{15}$  cm<sup>-3</sup>) on the size and density of the pores in a 4 M HF/DMSO solution at 2 mA/cm<sup>2</sup> for 60 min was investigated. The resulting morphologies are shown in Fig. 5. It can be seen that the pore diameter and the pore spacing decrease, whereas the pore number density increases with decreasing the substrate resistivity from 10-20 to 3.2-4.8  $\Omega$  cm (Fig. 5a and b). Furthermore, the thickness of the macropore walls is greatly reduced. The average pore wall thickness is about 800 nm in case of 10-20  $\Omega$  cm, reduced to around 150 nm on 3.2-4.8  $\Omega$  cm substrate. In general, the wall thickness is found to be smaller than the pore diameter at a specific resistivity. Square root dependence for the pore wall thickness with substrate doping density is reported.<sup>23</sup> Random pore distribution and dimensions and poorly defined pore morphology are obtained when the resistivity is reduced to 0.1-0.2  $\Omega$  cm, as shown in Fig. 5c. Meanwhile, if the substrate resistivity is reduced further to 0.01-0.02  $\Omega$  cm, only a homogeneous nanoporous layer is formed, as shown in Fig. 5d.

From these observations, it appears that there is a critical value of substrate resistivity (0.1-0.2  $\Omega$  cm in this study) below which no macropore can be formed. This phenomenon can be explained as a result of diminution of the passivating properties of the pore walls when the doping density exceeds a critical level, consistent with the improved version of the linear stability model.<sup>27</sup> Similar limiting value of resistivity was reported by another group in electrolytes containing organic solvents.<sup>33</sup> However, a limiting resistivity of around 5  $\Omega$  cm was found in aqueous solution.<sup>23</sup> The disappearance of macroporous structures on polished samples at a limiting resistivity depends not only on the electrolyte composition but also on the nature of the organic solvent.<sup>34</sup>

Based on these results, it is clear that high doping density substrates tend to form nanoporous layers rather than macropores. The influence of increasing the doping density on pore formation is similar to some extent to the influence of increasing the applied potential.

**Current density and anodization time.**—The effect of applied current density and anodization time on macropore formation and pore size were investigated. At constant current density the pore size increases with anodization time (time varied from 20 min up to 3 h).

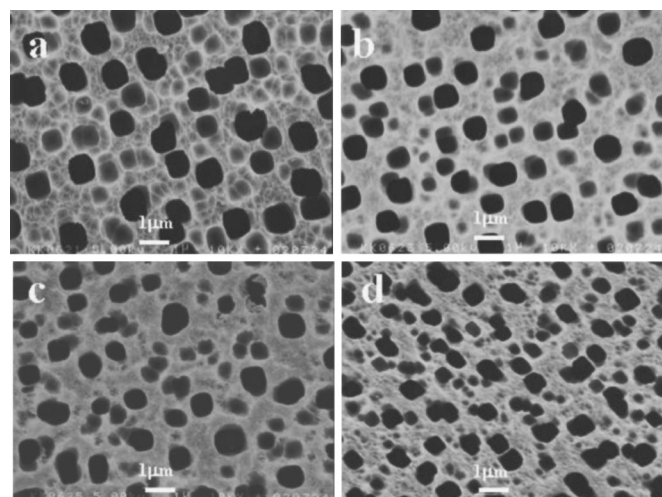


**Figure 6.** FE-SEM micrographs of macropores formed in a 10-20  $\Omega$  cm p-type Si in 4 M HF/DMSO at different current densities and various times: (a) 2 mA/cm<sup>2</sup> for 100 min, (b) 5 mA/cm<sup>2</sup> for 40 min, (c) 10 mA/cm<sup>2</sup> for 20 min, and (d) 50 mA/cm<sup>2</sup> for 4 min. The number of coulombs was 12 C/cm<sup>2</sup> in all cases.

As the anodization time increases, the interpore spacing decreases until the neighboring pores joined together, forming wider pores. The phenomenon of pore joining has been proposed by Lehmann and Föll.<sup>36</sup>

Figure 6 shows FE-SEM micrographs of the substrate anodized in a 4 M HF/DMSO at different current densities and various times. The number of coulombs was kept constant at 12 C/cm<sup>2</sup> in all cases. It can be observed that the pore size has no significant dependence on current density (it decreases slightly with increasing current density). The variation of pore growth rate (pore depth per time) with current density at the same quantity of charge was evaluated and the result is depicted in Fig. 7. The growth rate shows a linear dependence on current density. This result is in contrast with the case of

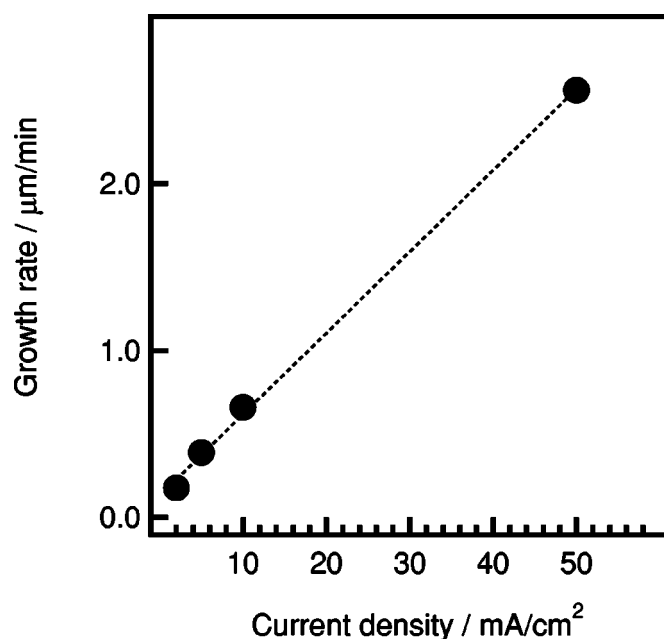


**Figure 7.** Pore growth rate as a function of applied current density for macropores obtained in 10-20  $\Omega$  cm p-type Si substrates in a 4 M HF/DMSO solution.

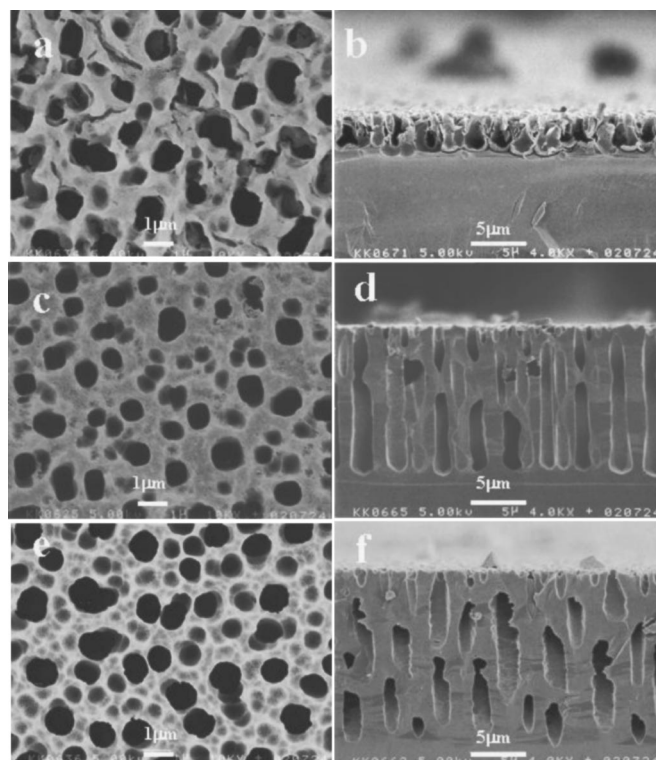


**Figure 8.** Top (left) and cross-sectional view (right) FE-SEM micrographs of macropores formed in 10-20  $\Omega$  cm p-type Si at 10 mA/cm<sup>2</sup> for 20 min in a DMSO solution with different HF concentrations: (a, b) 2 M, (c, d) 4 M, and (e, f) 10 M HF.

macropores prepared on n-type substrates, in which the growth rate is independent of current density.<sup>23</sup> Such increase with current density, however, is similar to the behavior of microporous silicon. At the same current density the growth rate is about two times greater than the growth rate of microporous structure, in agreement with the data reported in Ref. 23.

However, Vyatkin and co-workers<sup>37</sup> observed saturation in the growth rate of p-type macropores after a linear dependence with the current density. They used two different electrolytes of HF/DMF and HF/H<sub>2</sub>O/(CH<sub>3</sub>)<sub>2</sub>CHCO (10-20  $\Omega$  cm substrates) with a constant anodization time. They considered the leveling in growth rate as evidence that the charge-transfer process at the electrolyte/semiconductor interface is not anymore a limiting process for pore formation after exceeding a specific value of current density. Further, in this range of current density the etching rate should be controlled by a chemical reaction. Their observation is not contradictory to ours. Both results confirm that the growth rate is now not only dependent on the current density but also on the chemical composition of the electrolyte. This is further emphasized in the next section.

*Variation of HF concentration.*—The effect of changing HF concentration on pore morphology and depth was examined. Because the HF is prepared from an original 47 wt% HF solution, the electrolytes always include a certain amount of water (1 M HF solution contains about 1.1 M H<sub>2</sub>O). Top and cross-sectional view FE-SEM micrographs of macropores obtained at constant current density and time in a DMSO solution with 2, 4, and 10 M HF are shown in Fig. 8. At first sight it may seem that the resulting macropore of top-view images in Fig. 8a, c, and e have quite similar pore morphologies, and one may conclude that variation of HF concentration has no effect on macropore formation. On the contrary, drastic changes in both pore morphology and pore depth are clearly observed from cross-sectional views in Fig. 8b, d, and f. Unstable pore growth with the smallest growth rate is obtained in the solution

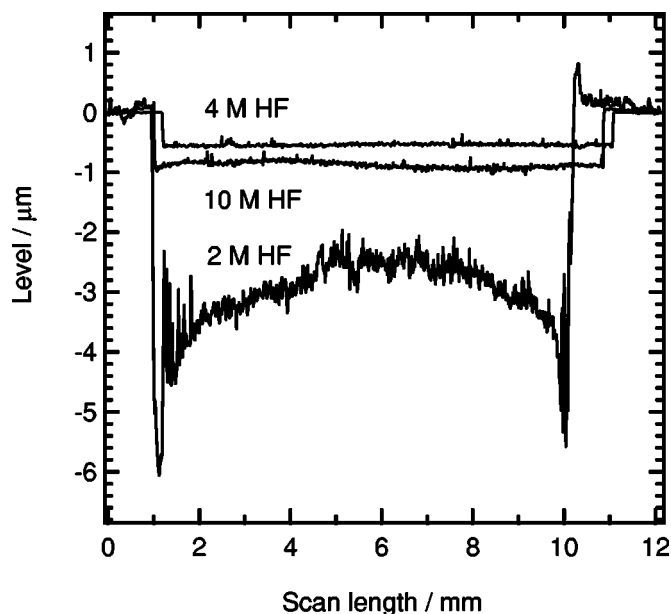


**Figure 9.** Topographic profiles of the macroporous structures prepared at  $10 \text{ mA/cm}^2$  for 20 min in a DMSO solution mixed with different HF concentrations.

with the 2 M HF. The observed pore depth after 20 min anodization at  $10 \text{ mA/cm}^2$  is only  $3.5 \mu\text{m}$ . At this low concentration of HF, the etching of pore walls is probably enhanced, which in turn gives a small aspect ratio (pore depth per diameter). Increasing the concentration of HF to 4 M improves the quality and stability of pore growth; the pore growth rate is greatly enhanced (a pore depth of about  $13 \mu\text{m}$  is obtained, Fig. 8d). When the HF concentration is further increased to 10 M, the reaction rate is a bit increased; the pore depth is developed to around  $15 \mu\text{m}$  (Fig. 8f). In both 4 and 10 M HF solutions, most of the pores are now empty.

Surface profiles of macropores prepared in different HF concentrations were performed. The profiles depicted in Fig. 9 depend on the HF concentration. In solution containing 2 M HF, the profile shows an average of a  $3 \mu\text{m}$  layer that etched away from the surface. The curvature of the profile is likely induced by stress.<sup>38</sup> The dissolution is greatly enhanced at the border of the macroporous area with the wafer; a similar result was observed for mesoporous structures in an earlier report.<sup>39</sup> However, when the HF concentration is increased to 4 or 10 M, mild dissolution occurs; around  $0.5\text{--}0.9 \mu\text{m}$  deep profiles are observed in both solutions. This means that 2 M HF content is the most aggressive solution.

Based on these results, it seems that there is a threshold concentration of HF below which unstable pore growth and very small aspect ratio are obtained. Under our own experimental conditions, the optimum concentration for stable macropore formation should not be below 4 M. The observed dependence of pore growth rate on HF concentration can be ascribed to different solution aggressiveness. There is general agreement that the HF concentration in the electrolyte determines the critical current density of porous layer formation ( $J_{\text{PSL}}$ ). This means that the effects of changing HF and current density on reaction rate resemble each other. This confirms again that the electrochemical reaction associated with the pore formation is not only dependent on current density and semiconductor properties but also on the electrolyte composition.

**Impregnation with Ag metal.**—The behavior of macropores formed using  $10\text{--}20 \Omega \text{ cm}$  substrate in a DMSO solution in contact with  $\text{Ag}^+$  ions (at OCP, 60 min, in the dark, room temperature) is investigated. Figure 10 shows top and cross-sectional view FE-SEM micrographs obtained after immersion in a  $5 \times 10^{-3} \text{ M Ag}_2\text{SO}_4$

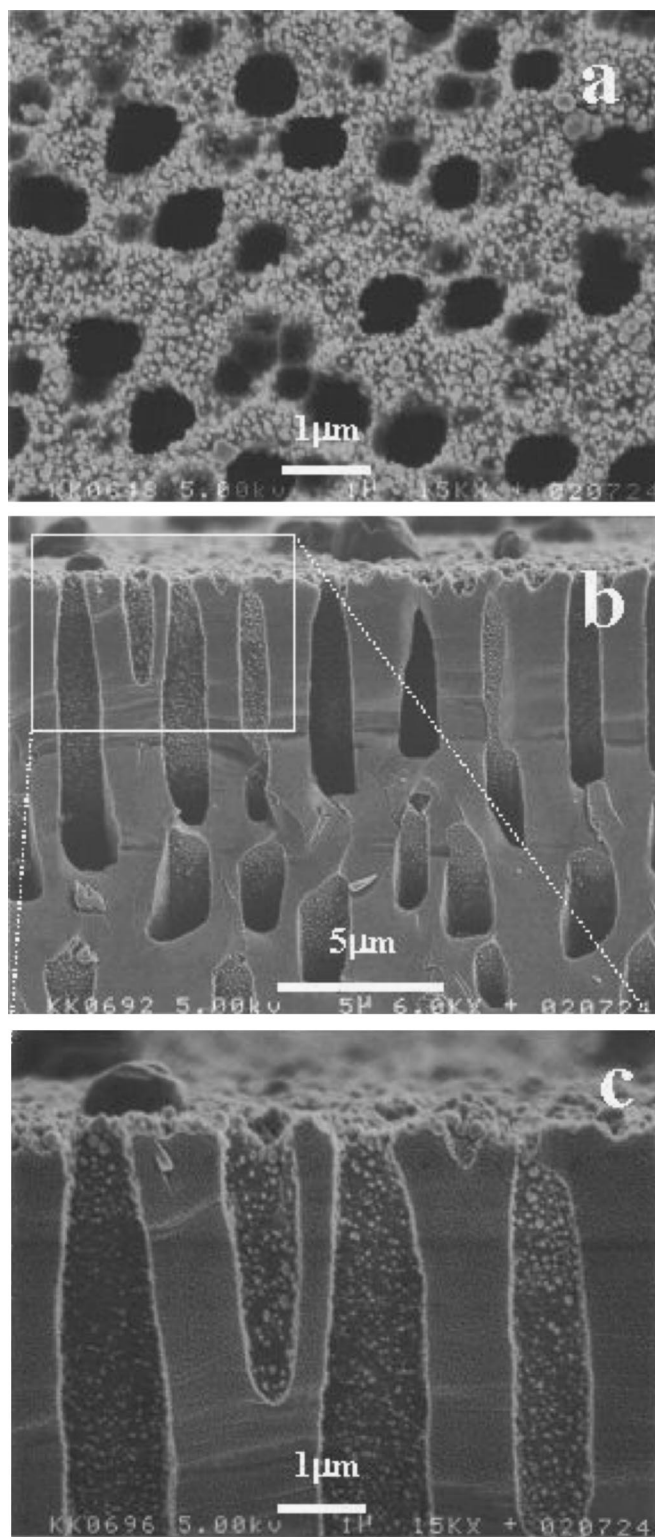


**Figure 10.** FE-SEM images of macropores after immersion plating in  $5 \times 10^{-3} \text{ M Ag}_2\text{SO}_4$  for 60 min in the dark and at room temperature: (a) top-view, and (b) cross-sectional view, and (c) cross-sectional view at a higher magnification. The macropores are formed in a  $10\text{--}20 \Omega \text{ cm}$  p-type Si at  $10 \text{ mA/cm}^2$  for 10 min in a solution composed of 4 M HF/DMSO.

aqueous solution. As shown in the images, Ag particles with a size in the range of  $50 \text{ nm}$  are clearly observed on the entire surface of macropores (both on the top surface and deep inside the pores). This result indicates that there is no great problem of mass transport

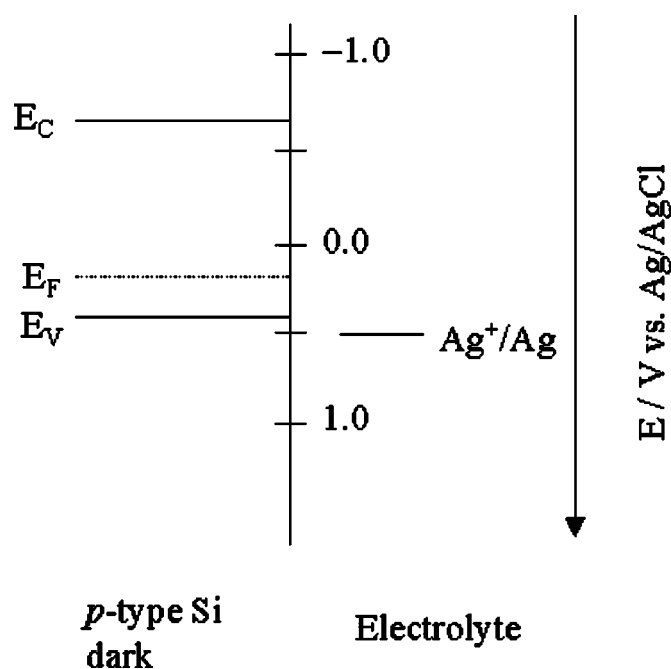


**Figure 11.** Schematic representation of energy band diagram for a p-type Si (in the dark) in contact with  $5 \times 10^{-3}$  M  $\text{Ag}_2\text{SO}_4$  solution, illustrating the energetic position of the bandedges with respect to the equilibrium potential of the redox couple.

inside the pores, which may limit the deposition process. In other words,  $\text{Ag}^+$  ions easily diffuse into the pores and thereby the reduction immediately takes place. According to this observation, it is concluded that the macropore prepared in p-type Si can be used as a host matrix to introduce noble metals deep into the pores by impregnating the pores in an appropriate immersion plating solution.

Now a question arises to understand the reaction mechanism involved during the deposition process. We used a p-type electrode and the deposition is observed at the open-circuit potential (OCP) in the dark. This means that the reaction mechanism most likely proceeds by hole injection from  $\text{Ag}^+$  ion solution to the valence band of the silicon. To clarify the possibility of this mechanism, the energy band diagram for a p-type Si in contact with the  $\text{Ag}^+$ -containing solution is determined. Our calculations are based on the following assumptions: (i) the redox potential of  $\text{Ag}^+/\text{Ag}$  is calculated as 0.47 V vs.  $\text{Ag}/\text{AgCl}$  for  $5 \times 10^{-3}$  M metal ions in solution; (ii) under equilibrium conditions, the Fermi level in the semiconductor is represented by the electrode potential (OCP),<sup>40</sup> which was measured in the dark, and the value was taken during the initial stage of immersion (0.17 V vs.  $\text{Ag}/\text{AgCl}$ ); (iii) for a p-Si (doping density  $10^{15} \text{ cm}^{-3}$ ) the Fermi level ( $E_F$ ) is located 0.24 V above the position of the valence bandedge ( $E_V$ ); i.e.,  $E_F - E_V = 0.24 \text{ V}$ ;<sup>41</sup> (iv) the Si bandedges are fixed.

The resulting simplified band model for the reduction of  $\text{Ag}^+$  ions at the Si surface is illustrated in Fig. 11 at its flatband condition. As can be seen, the  $\text{Ag}$  redox level has a good overlap with the valence bandedge of Si; it has a more positive potential than the position of the valence bandedge. Consequently, hole injection from the ions in solution to the valence band of Si is energetically favorable, and deposition does occur at the OCP, as is already observed experimentally. Hole injection leads to oxidation of the macroporous substrate. Surface oxidation is indeed observed and detected by Fourier transform infrared (FTIR) spectra (not shown here). Accordingly, the deposition of  $\text{Ag}$  from  $\text{Ag}_2\text{SO}_4$  can be represented by the following redox couple

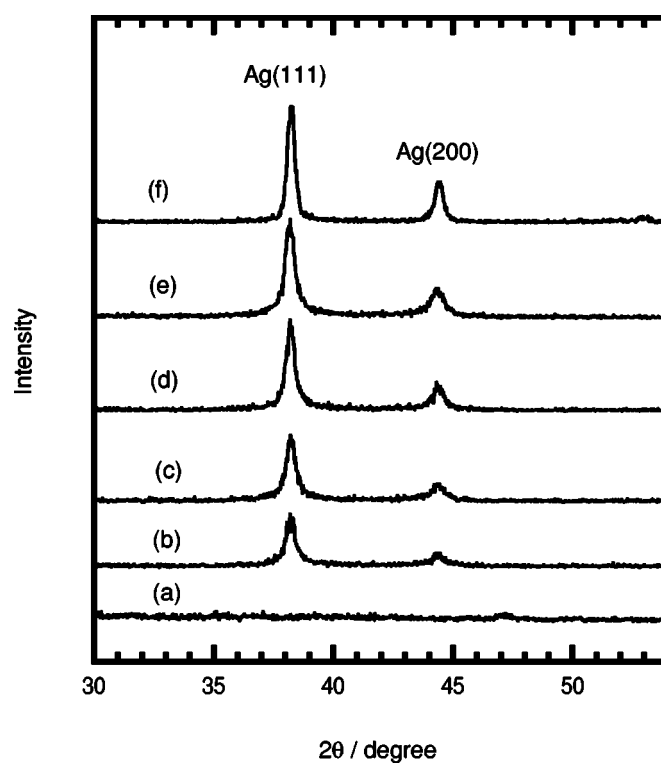


**Figure 12.** XRD patterns for macropores prepared in 10-20 nm p-type Si substrates after immersion in  $5 \times 10^{-3}$  M  $\text{Ag}_2\text{SO}_4$  in the dark at different times: (a) 0, (b) 1, (c) 2, (d) 5, (e) 20, and (f) 60 min.



As a last comment, the crystallinity of  $\text{Ag}$  deposits on the macroporous surface is analyzed with XRD at different deposition times. The result is shown in Fig. 12. The patterns exhibit two peaks at  $38.2^\circ$  and  $44.4^\circ$ , corresponding, respectively, to  $\text{Ag}(111)$  and  $\text{Ag}(200)$ . The peak intensity for both phases increases with immersion time (Fig. 10b-f). Assuming that the  $\text{Ag}$  particles are stress-free, the average crystallite size can be estimated by applying the Scherrer equation<sup>42</sup>

$$D = C\lambda/\beta \cos \theta$$

where  $\lambda$  is the X-ray wavelength (nm),  $\beta$  is the full width at half maximum (fwhm) of the peak (radians),  $\theta$  is Bragg angle,  $C$  is a factor (typically from 0.9 to 1.0) depending on crystallite shape, and  $D$  is the crystallite size (nm). For the  $\text{Ag}(111)$  peak of Fig. 12f, average particle size was found to be 42 nm and for the (200) peak the value was 43 nm. These values are close and in good agreement with the average size detected from FE-SEM images in Fig. 10.

From this result, it is concluded that macroporous structure can be used as a host matrix for metal deposition into the pores. For any metal/metal ion redox couple with a more positive equilibrium potential than the valence bandedge, the deposition can take place in the dark by a simple immersion plating method.

### Conclusions

To better understand the role of different factors affecting the macropore formation in p-type Si substrates, we have performed a series of experimental investigations in HF-containing organic electrolytes. The results led to some important conclusions:

1. The presence of an organic solvent plays an essential role for better pore formation.

2. A nanoporous layer is observed in the MeCN-containing solution. In case of DMSO or DMF solutions, this nanoporous layer is most likely formed and consequently etched away.

3. Filled macroporous structures obtained with nanoporous body in the MeCN solution indicate that the current density at the pore tip is far from the electropolishing regime.

4. Macropores are observed for a limiting substrate resistivity of 0.1-0.2  $\Omega$  cm. For higher doping density, only nanoporous layers are formed due to a loss of the passivating character of the pore walls.

5. The content of HF in solution is critical for the dissolution process. An appropriate concentration should be added to control the pore morphology and the growth velocity.

6. The pores grow perpendicularly on the substrate surface and follow the  $\langle 100 \rangle$  direction. The macropore growth rate has a linear dependence on current density, and the value is found to be about two times greater than that of the microporous silicon.

7. The pore size and spacing decrease with decreasing the substrate resistivity, however they have insignificant dependence on current density.

8. Finally, as-prepared macroporous structure has been successfully used as a host matrix for Ag deposition at the OCP without using any catalytic treatment or external bias. The crystallinity of Ag deposits is confirmed and the reaction mechanism is clarified. Generally, for any metal/metal ion couples with energy levels that overlap with the valence bandedge, open-circuit deposition is expected to occur in the dark via injection of holes from the metal ion solution to the valence band.

#### Acknowledgments

The authors thank D. Hamm of Kyoto University for valuable discussion and Y. Mizutani and T. Nagayama of Kyoto Municipal Institute for Industrial Research for their support during FE-SEM observation. This research was partly supported by a Grant-in-Aid from the Ministry of Education, Culture, Sports, Science and Technology. F.A.H. acknowledges support from the Japan Society for the Promotion of Science in the form of a JSPS postdoctoral fellowship.

*Kyoto University assisted in meeting the publication costs of this article.*

#### References

1. A. Uhler, *Bell Syst. Tech. J.*, **35**, 333 (1956).
2. D. R. Turner, *J. Electrochem. Soc.*, **105**, 402 (1958).
3. R. L. Smith and S. D. Collins, *J. Appl. Phys.*, **71**, R1 (1992).
4. A. G. Cullis, L. T. Canham, and P. D. J. Calcott, *J. Appl. Phys.*, **82**, 909 (1997).
5. V. Lehmann, W. Honlein, R. Reisinger, A. Spitzer, H. Wendt, and J. Willer, *Thin Solid Films*, **276**, 138 (1996).
6. S. Ottow, V. Lehmann, and H. Föll, *J. Electrochem. Soc.*, **143**, 385 (1996).
7. H. Ohji, P. T. J. Gennissen, P. J. French, and K. Tsutsumi, *J. Micromech. Microeng.*, **10**, 440 (2000).
8. R. Angelucci, A. Poggi, L. Dori, G. C. Cadinali, A. Parisini, A. Tagliani, M. Mariasaldi, and F. Cavani, *Sens. Actuators, A*, **74**, 1 (1999).
9. C. M. A. Ashruf, P. J. French, P. M. Sarro, R. Kazinczi, X. H. Xia, and J. J. Kelly, *J. Micromech. Microeng.*, **10**, 505 (2000).
10. V. Lehmann, *Electrochemistry of Silicon*, p. 223, Wiley-VCH, Weinheim (2002).
11. V. Lehmann and S. Rönnebeck, *Sens. Actuators, A*, **95**, 202 (2001).
12. E. A. Ponomarev and C. Lévy-Clément, *J. Porous Mater.*, **7**, 51 (2000).
13. C. Lévy-Clément, S. Lust, S. Bastide, Q. N. Lê, and D. Sarti, *Phys. Status Solidi A*, **197**, 27 (2003).
14. U. Grüning, S. Ottow, and V. Lehmann, *Appl. Phys. Lett.*, **68**, 747 (1996).
15. S. R. Nicewarner-Pena, R. G. Freeman, B. D. Reiss, L. He, D. J. Pena, I. D. Walton, R. Cromer, C. D. Keating, and M. J. Natan, *Science*, **294**, 137 (2001).
16. M. J. J. Theunissen, *J. Electrochem. Soc.*, **119**, 351 (1972).
17. V. Lehmann, *J. Electrochem. Soc.*, **140**, 2836 (1993).
18. V. Lehmann and U. Grüning, *Thin Solid Films*, **297**, 13 (1997).
19. E. K. Propst and P. A. Kohl, *J. Electrochem. Soc.*, **141**, 1006 (1994).
20. R. B. Wehrspohn, J.-N. Chazalviel, F. Ozanam, and I. Solomon, *Thin Solid Films*, **297**, 5 (1997).
21. E. A. Ponomarev and C. Lévy-Clément, *Electrochem. Solid-State Lett.*, **1**, 42 (1998).
22. P. C. Seanson, J. M. Macaulay, and F. M. Ross, *J. Appl. Phys.*, **72**, 253 (1992).
23. V. Lehmann and S. Rönnebeck, *J. Electrochem. Soc.*, **146**, 2968 (1999).
24. R. B. Wehrspohn, J.-N. Chazalviel, and F. Ozanam, *J. Electrochem. Soc.*, **145**, 2958 (1998).
25. J. Carstensen, M. Christophersen, and H. Föll, *Mater. Sci. Eng., B*, **69-70**, 23 (2000).
26. E. S. Kooij and D. Vanmaekelbergh, *J. Electrochem. Soc.*, **144**, 1296 (1997).
27. J.-N. Chazalviel, F. Ozanam, N. Gabouze, S. Fellah, and R. B. Wehrspohn, *J. Electrochem. Soc.*, **149**, C511 (2002).
28. F. A. Harraz, K. Kamada, J. Sasano, S. Izuo, T. Sakka, and Y. H. Ogata, *Phys. Status Solidi A*, In Press.
29. J. Carstensen, R. Prange, and H. Föll, *J. Electrochem. Soc.*, **146**, 1134 (1999).
30. M. Christophersen, J. Carstensen, S. Rönnebeck, C. Jäger, W. Jäger, and H. Föll, *J. Electrochem. Soc.*, **148**, E267 (2001).
31. J. H. Song and M. J. Sailor, *Inorg. Chem.*, **37**, 3355 (1998).
32. F. A. Harraz, T. Sakka, and Y. H. Ogata, *Electrochim. Acta*, **46**, 2805 (2001).
33. S. Lust and C. Lévy-Clément, *J. Electrochem. Soc.*, **149**, C338 (2002).
34. S. Lust and C. Lévy-Clément, *Phys. Status Solidi A*, **182**, 17 (2000).
35. S. M. Sze, *Semiconductor Devices: Physics and Technology*, 2nd ed., p. 428, Wiley & Sons, Inc., New York (2002).
36. V. Lehmann and H. Föll, *J. Electrochem. Soc.*, **137**, 653 (1990).
37. A. Vyatkin, V. Starkov, V. Tzeitlin, H. Presting, J. Konle, and U. König, *J. Electrochem. Soc.*, **149**, G70 (2002).
38. J. M. Lopez-Villegas, M. Navarro, D. Papadimitriou, J. Basses, and J. Samitier, *Thin Solid Films*, **276**, 238 (1996).
39. D. Hamm, J. Sasano, T. Sakka, and Y. H. Ogata, *J. Electrochem. Soc.*, **149**, C331 (2002).
40. R. Memming, *Semiconductor Electrochemistry*, p. 104, Wiley, Weinheim (2001).
41. S. M. Sze, *Physics of Semiconductor Devices*, 2nd ed., p. 26, Wiley, New York (1981).
42. H. P. Klug and L. E. Alexander, *X-Ray Diffraction Procedures for Polycrystalline and Amorphous Materials*, p. 540, Wiley-Interscience, New York (1974).